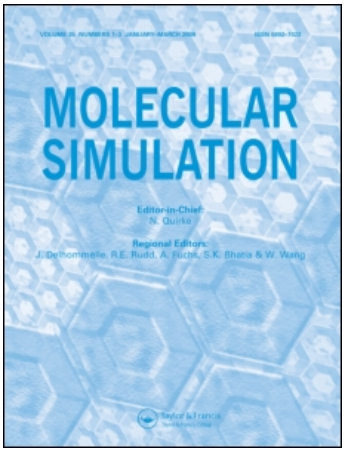

Molecular Simulation
Publication details, including instructions for authors and subscription information:
http://www.informaworld.com/smpp/title~content=t713644482

FT-IR, FT-Raman and UV-vis spectra and quantum chemical investigation of carvedilol

Lakshmi Jagannathan[a]; R. Meenakshi[a]; S. Gunasekaran[b]; S. Srinivasan[c]
[a] Department of Physics, C.T.T.E. College for Women, Chennai, India [b] PG and Research Department of Physics, Pachaiyappa's College, Chennai, India [c] Department of Physics, L.N. Government College, Ponneri, India

First published on: 08 October 2009

To cite this Article Jagannathan, Lakshmi , Meenakshi, R. , Gunasekaran, S. and Srinivasan, S.(2010) 'FT-IR, FT-Raman and UV-vis spectra and quantum chemical investigation of carvedilol', Molecular Simulation, 36: 4, 283 — 290, First published on: 08 October 2009 (iFirst)
To link to this Article: DOI: 10.1080/08927020903313998
URL: http://dx.doi.org/10.1080/08927020903313998

Molecular Simulation
Vol. 36, No. 4, April 2010, 283–290

Taylor & Francis
Taylor & Francis Group

FT-IR, FT-Raman and UV–vis spectra and quantum chemical investigation of carvedilol

Lakshmi Jagannathan[a], R. Meenakshi[a], S. Gunasekaran[b1] and S. Srinivasan[c]*

[a]*Department of Physics, C.T.T.E. College for Women, Chennai 600 011, India;* [b]*PG and Research Department of Physics, Pachaiyappa's College, Chennai 600 030, India;* [c]*Department of Physics, L.N. Government College, Ponneri 601 204, India*

(*Received 24 June 2009; final version received 7 September 2009*)

The FT-IR and FT-Raman spectra of carvedilol were recorded in the regions 4000–400 and 3500–100 cm^{-1}, respectively. The electronic absorption spectrum was recorded in the region 400–200 nm. In the present study, AM1 and PM3 semi-empirical molecular orbital methods were employed to study molecular structure as well as to predict infrared spectra. The AM1-optimised geometry was used in the density functional theory (DFT) calculation to predict the oscillator strength, electronic transition energies between the orbitals and wavelength of the transitions. The DFT-based NMR calculation procedure was used to assign the ^1H NMR chemical shift of carvedilol. The electron density-based local reactivity descriptors such as Fukui functions were calculated to explain the chemical selectivity or reactivity site in carvedilol.

Keywords: carvedilol; FT-IR; FT-Raman; UV spectra; NMR chemical shift

1. Introduction

Carvedilol, 1-(9H-carbazol-4-yloxy)-3-[2-(2-methoxy-phenoxy)ethyl amino]-2-propanol ($C_{24}H_{26}N_2O_4$), is a lipophilic multiple action neurohormonal antagonist [1]. As a β-blocker, carvedilol reduces the total cardiac workload [2,3]. Therapeutically, carvedilol is a cardio-vascular drug of proven efficiency in the treatment of mild to moderate congestive heart failure, essential hypertension, angina and in the improvement of the left ventricular function [4]. It was synthesised by Wiedemann et al. [5], but they did not report the crystal structure. Chen et al. [6] discussed the X-ray crystallographic study of the carvedilol synthesised by Wiedemann et al. [5] in order to understand the mechanism of the action on the receptor. Oliveira et al. [7] carried out theoretical studies to determine the relevance of conformation and proton affinity of the protonable amino side-chain group in the proton shuttling activity across the inner mitochondrial membrane. The pH-dependent Raman spectroscopic studies of carvedilol in both solid samples and DMSO solutions were studied by Marques et al. [8]. Carvedilol has been analysed with NMR spectroscopy (in DMSO) to correlate theoretically and experimentally derived electronic structure [9]. Almeida et al. [10] studied the enantiometric relationships of carvedilol fragment 4-(2-hydroxypropoxy)carbazol, along with its analogues recently. Also, the conformational-dependent basicity of carvedilol fragment 2(*S*)-1-(ethylammonium)propane-2-ol and aminoethoxy-2-methoxy-benzene has been made through *ab initio* methods [11,12]. Hence, the title molecule is of considerable interest in the field of medicinal and pharmaceutical science. The present study is devoted to performing a detailed calculation of the molecular structure as well as to predicting the infrared, UV spectra, ^1H NMR chemical shifts and chemical reactivity sites of the title molecule.

2. Experimental methods

The spectroscopic pure sample of carvedilol was procured from reputed pharmaceutical firms in Chennai, India and used as such. The Fourier transform infrared spectrum of carvedilol was recorded with an ABB Bomem Series spectrometer over the region 4000–400 cm^{-1} by adopting the KBr pellet technique at Dr Ceeal Analytical Lab, Chennai, India. The FT-Raman spectrum was recorded at Central Electro Chemical Research Laboratory, Karaikudi, India using a Nexus 670 spectrometer. A laser frequency of 15,798 cm^{-1} was used as an excitation source. The spectrometer is fitted with an XT-KBr beam splitter and a DTGS detector. A baseline correction was made for the spectrum recorded. The UV–vis spectral measurements were carried out using a Shimadzu-160A spectrometer at Dr Ceeal Analytical Lab.

3. Computation details

The computations were performed with the GAUSSIAN 03W [13] package, with semi-empirical molecular orbital and density functional methods. The equilibrium geometries of the molecule were determined by the gradient technique. The force constants and vibrational frequencies were determined by the FREQ calculations on the stationary points obtained after the optimisation to verify if there were true minima. The ZINDO and time-dependent

*Corresponding author. Email: dr_s_srinivasan@yahoo.com

ISSN 0892-7022 print/ISSN 1029-0435 online

DOI: 10.1080/08927020903313998
http://www.informaworld.com

density functional theory (TD-DFT) methods were used for the calculation of the UV–vis spectra. The IR and UV–vis spectra were calculated and visualised using the SWizard program [14]. The ^{1}H NMR chemical shifts of the title compound were calculated using the keyword NMR in the DFT calculation at the B3LYP level with 6-31G (d,p) basis set. The chemically active sites for nucleophilic and electrophilic attack for carvedilol were calculated using the methodology of Kolandaivel et al. [15].

4. Results and discussion

4.1 Molecular geometry

The optimised geometry of carvedilol, obtained at the AM1 and PM3 levels of calculation, is provided in Tables 1 and 2 in accordance with the atom numbering scheme given in Figure 1. Tables 1 and 2 compared the bond lengths and bond angles, respectively, for carvedilol with those experimentally available from X-ray diffraction data [6]. From the calculated values, we can find that most of the optimised bond lengths are slightly larger than the experimental values, due to this the theoretical calculation belongs to the isolated molecules in the gaseous phase whereas the experimental results belong to the molecules in the solid phase. Comparing bond lengths and bond angles of the AM1 result with PM3, as a whole, the former is smaller than the latter and the AM1-calculated values correlate fairly compared with the experimental results. Although it has slight differences, calculated geometric parameters represent a good approximation, and they are the base for calculating other parameters, such as vibrational frequencies, NMR chemical shifts, atomic charges, etc.

4.2 Vibrational band assignment

Carvedilol minimum energy structure belongs to the C_1 symmetry point group. We have assigned the fundamental modes of these groups on the basis of group vibrational concept and calculated vibrational frequencies. Figures 2 and 3 show the FT-IR and FT-Raman spectra of carvedilol, respectively. The principal peaks are provided in Table 3. From Table 3, we can see that the best representation of the IR spectrum is obtained with all the methods in the low-frequency region. From Table 3, both AM1 and PM3 produce the same result and agree with the experimental values.

Table 1. Selected bond length values for carvedilol.

Bond length (Å)	AM1	PM3	Exp[a]	Bond length (Å)	AM1	PM3	Exp[a]	Bond length (Å)	AM1	PM3	Exp[a]
C_1—C_2	1.533	1.546	1.514	C_{13}—C_{14}	1.393	1.39	1.408	C_{24}—C_{25}	1.45	1.453	1.437
C_2—C_3	1.543	1.544	1.518	C_{14}—C_9	1.402	1.4	1.371	C_{25}—C_{26}	1.388	1.39	1.398
C_2—O_4	1.417	1.413	1.43	C_{10}—O_{15}	1.387	1.393	1.365	C_{26}—C_{27}	1.395	1.39	1.374
C_3—N_5	1.441	1.477	1.459	O_{15}—C_{16}	1.429	1.411	1.429	C_{27}—C_{28}	1.399	1.398	1.385
N_5—C_6	1.451	1.484	1.462	C_1—O_{17}	1.433	1.429	1.431	C_{28}—C_{29}	1.394	1.39	1.362
C_6—C_7	1.534	1.533	1.497	O_{17}—C_{23}	1.381	1.389	1.372	C_{29}—C_{30}	1.397	1.392	1.384
C_7—O_8	1.44	1.421	1.424	N_{18}—C_{19}	1.407	1.435	1.374	C_{30}—N_{18}	1.41	1.435	1.382
O_8—C_9	1.387	1.391	1.368	C_{19}—C_{20}	1.4	1.393	1.391	N_{18}—H_{49}	0.987	0.991	
C_9—C_{10}	1.408	1.408	1.394	C_{20}—C_{21}	1.391	1.39	1.363	O_4—H_{36}	0.967	0.948	
C_{10}—C_{11}	1.402	1.399	1.37	C_{21}—C_{22}	1.398	1.396	1.395	N_5—H_{37}	1.004	0.999	
C_{11}—C_{12}	1.392	1.39	1.357	C_{22}—C_{23}	1.401	1.399	1.383				
C_{12}—C_{13}	1.396	1.392	1.36	C_{23}—C_{24}	1.399	1.398	1.394				

[a] Ref. [6].

Table 2. Selected bond angle values for carvedilol.

Bond angle (°)	Exp[a]	AM1	PM3	Bond angle (°)	Exp[a]	AM1	PM3	Bond angle (°)	Exp[a]	AM1	PM3
C_1—C_2—C_3	110.4	109.1	109	C_{12}—C_{13}—C_{14}	119.9	120.4	120.5	C_{24}—C_{19}—N_{18}	108.5	109.5	109.4
C_2—C_3—N_5	112.4	116.8	115.7	C_{14}—C_9—C_{10}	125.1	119.9	119.8	N_{18}—C_{30}—C_{25}	108	109.5	109.5
C_3—N_5—C_6	111.7	114.3	115	C_{10}—O_{15}—C_{16}	117.9	113.9	113.3	C_{19}—N_{18}—C_{30}	109.1	107.6	106.1
N_5—C_6—C_7	111.4	111.9	109.3	C_2—C_1—O_{17}	106.8	104.9	106.4	C_{24}—C_{25}—C_{30}	106.8	106.4	107.2
C_6—C_7—O_8	106.3	104.7	111.9	C_1—O_{17}—C_{23}	118.9	116	112.6	C_{25}—C_{26}—C_{27}	119	118.8	118.3
C_7—O_8—C_9	118.4	113.1	114.4	C_{23}—C_{22}—C_{21}	119.6	120.3	120.4	C_{26}—C_{27}—C_{28}	120.9	121.1	121.3
C_9—C_{10}—C_{11}	120	119.9	119.9	C_{22}—C_{21}—C_{20}	122.7	122.2	121.6	C_{27}—C_{28}—C_{29}	121.8	121.7	121.4
C_{10}—C_{11}—C_{12}	119.9	119.7	119.7	C_{21}—C_{20}—C_{19}	117.4	117.8	117.7	C_{28}—C_{29}—C_{30}	117.7	117.8	117.5
C_{11}—C_{12}—C_{13}	121.3	120.4	120.4	C_{19}—C_{24}—C_{23}	119.5	119	118.7				

[a] Ref. [6].

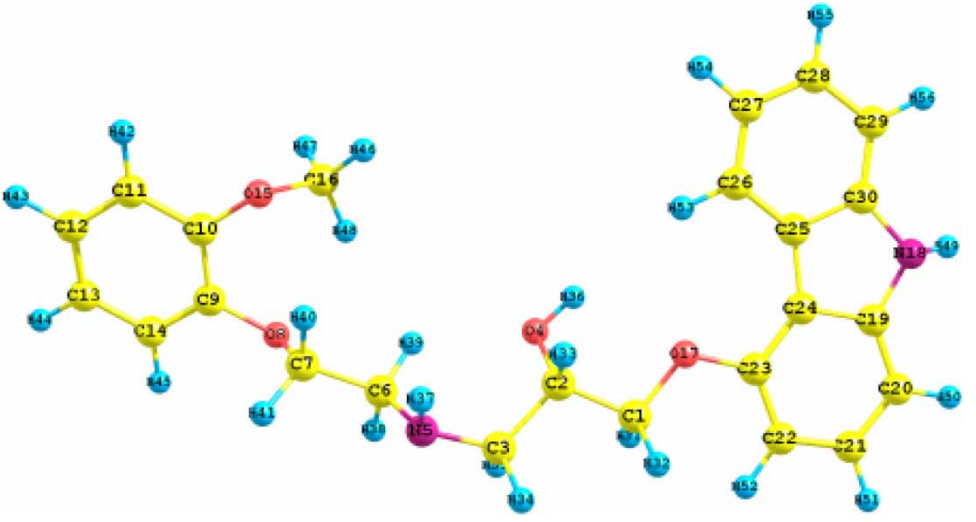

Figure 1. Atom numbering adopted in this study for carvedilol.

4.2.1 *N—H vibration*

In general, N—H stretching vibration occurs in the region 3500–3000 cm^{-1}. Bayari et al. [16] assigned the band at 3364 cm^{-1}, which corresponds to N—H stretching in methylphenitate. Also, Krishnakumar and Seshadri [17] assigned the N—H stretching vibration at 3245 cm^{-1} in 2-methylpiperazine. Chithambarathanu et al. [18] made an assignment of N—H stretching at 3321 cm^{-1} in 2,6-di(*p*-methoxy phenyl)-3-methyl piperidone. Hence, in the present study, a weak band at 3467 cm^{-1} in FT-IR and 3359 cm^{-1} was assigned to the N—H stretching vibrational mode. This assignment was made by analogy with the earlier reports [16–18].

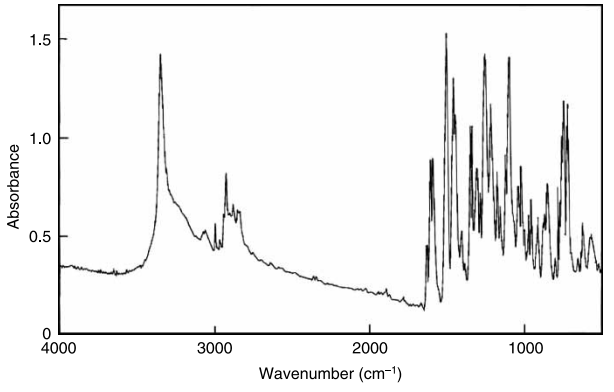

Figure 2. FT-IR spectrum of carvedilol.

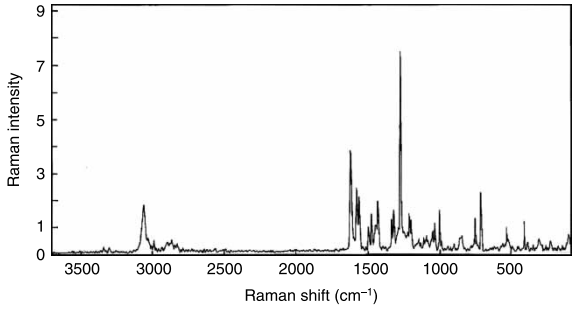

Figure 3. FT-Raman spectrum of carvedilol.

4.2.2 *C—H vibration*

The hetero-aromatic structure shows the presence of C—H stretching vibrations in the region 3100–3000 cm^{-1}, which is the characteristic region for the ready identification of the C—H stretching vibrations [19]. In this region, the bands are not affected appreciably by the nature of the substitutions. Hence, in the present work, the observed bands at 2959, 2987 and 3066 cm^{-1} in FT-IR and 2914, 2989 and 3065 cm^{-1} in the FT-Raman spectrum are assigned to C—H stretching vibration for carvedilol. In general, the calculated C—H stretching vibrations associated with the phenyl ring appeared at the higher wavenumber and C—H stretching vibrations associated with methylene and methyl groups appeared at the lower wavenumber. The aromatic C—H vibrations calculated theoretically are in good agreement with the experimentally reported values [20]. The title molecule has out-of-plane and in-plane aromatic bending vibrations that are found well within the experimentally predicted region. The out-of-plane bending mode of vibrations lies within the experimentally predicted region of 910–850 cm^{-1} [21], coinciding satisfactorily at both AM1- and PM3-calculated values. The bands corresponding to in-plane C—H deformations are observed in the region 1000–1300 cm^{-1}. The bands are sharp but of weak to minimum intensity. The medium and strong intensity bands at 1100, 1120, 1156 and 1177 cm^{-1} in the FT-IR spectrum, and

Table 3. Observed and calculated IR wavenumbers for carvedilol.

No.	FT-IR	FT-Raman	AM1	PM3	Assignment
1	–	115	119	121	CNC out-of-plane bending
2	–	245	236	247	CCN out-of-plane bending
3	–	329	310	332	C—CH_3 in-plane bending/CNC in-plane bending
4	–	402	423	407	CCN in-plane bending
5	–	426	437	423	CC out-of-plane bending/CO out-of-plane bending
6	510	–	506	507	CCC out-of-plane bending
7	536	550	544	537	CCC out-of-plane bending/CO in-plane bending
8	565	–	582	568	CCC out-of-plane bending
9	620	–	620	632	CCO in-plane bending
10	728	726	710	715	C—OH bending
11	747	–	–	–	CCC in-plane bending
12	759	–	–	–	CCC in-plane bending
13	770	769	777	769	CH_3 wagging/CCC in-plane bending
14	784	–	784	782	CCC in-plane bending
15	798	–	789	795	CCC ring breathing
16	805	–	812	821	CCC ring breathing
17	850	–	855	846	CH out-of-plane bending
18	857	862	865	851	CH out-of-plane bending
19	871	–	–	886	CH out-of-plane bending
20	880	–	884	889	CH out-of-plane bending
21	915	913	917	913	CH out-of-plane bending
22	957	–	960	957	C—CH_2 stretching
23	1022	1012	995	992	CH out-of-plane bending
24	1041	1047	1000	1001	CH_3 rocking
25	–	1064	1099	1045	CN out-of-plane bending/CH_2 twisting
26	1100	1110	1112	1101	CH in-plane bending
27	1120	1124	1127	1120	CH in-plane bending
28	1156	1160	1156	1152	CH in-plane bending
29	1177	–	1177	1171	CH in-plane bending
30	1215	1214	1218	1212	C–CH_3 stretching/CH in-plane bending
31	1224	1224	1223	–	CH_2 twisting
32	1256	–	1268	1264	CC stretching
33	1286	1285	1286	1290	CC stretching
34	1305	–	1308	1302	CH_2 wagging
35	1334	1333	1326	1336	CH in-plane bending
36	1348	1347	1349	1345	CC stretching
37	1403	–	1402	1403	CC stretching
38	1444	1444	1447	1444	CN stretching
39	1454	1489	1453	–	CN stretching/CH_3 deformation
40	1502	1509	1495	1518	C═C stretching
41	–	1574	1571	1558	C═C stretching
42	1591	1591	–	–	C═C stretching
43	1608	–	1608	1613	C═C stretching
44	1631	1631	1648	1645	CO stretching/CC stretching
45	2850	–	–	2811	CH stretching
46	2878	2875	–	–	CH stretching
47	2923	–	2959	2914	CH stretching
48	2996	2996	2987	2989	CH stretching
49	3061	3065	3066	3065	CH stretching
50	3307	–	3467	3359	NH stretching
51	3344	–	3517	3431	OH stretching

at 1110, 1124 and 1160 cm^{-1} in the FT-Raman spectrum for carvedilol are due to the C—H in-plane bending vibrations. The theoretically computed values of C—H in-plane bending also fall in the region mentioned above by both AM1 and PM3 methods. The C—H bending vibrations in the methyl and methylene groups were identified and assigned (Table 3).

4.2.3 Phenyl ring vibration

The benzene ring modes predominantly involve C—C bonds. A medium experimental peak around 1256–1403 cm^{-1} in FT-IR and FT-Raman was assigned to C—C stretching vibrations. The calculated wavenumbers also agree closely with the experimental results. The bands in the region 1502–1608 cm^{-1} observed in both FT-IR and

FT-Raman were assigned to C=C stretching vibrations. For a number of *meta*-, *ortho*- and *para*-substituted benzenes, the ring breathing mode is assigned at 1040–800 cm^{-1}, respectively [22–24]. In the present case, the bands observed at 805 and 798 cm^{-1} in FT-IR are assigned to the ring breathing mode. The theoretically predicted wavenumber at 789 and 812 cm^{-1} by the AM1 method and at 795 and 821 cm^{-1} by the PM3 method closely coincides with the experimental observation. However, the FT-Raman experimental observation shows that no such vibration would exist. The CCC in-plane and out-of-plane bending vibrations are also identified and presented in Table 3.

4.2.4 C—N vibration

The identification of C—N vibrations is a very difficult task, since mixing of several bands is possible in the region. Silverstein et al. [25] assigned the C—N stretching vibrations in the region 1382–1266 cm^{-1}. In the present work, a weak band at 1444 cm^{-1} and a strong band at 1454 cm^{-1} in FT-IR and a strong band at 1444 and 1489 cm^{-1} in FT-Raman have been assigned to C—N stretching vibrations coupled with C—H deformations. The theoretically computed value matches closely with the experimental values.

The bands of medium intensity at 115 and 245 cm^{-1} observed in FT-Raman may be due to the CNC and CCN bending vibrations, respectively, which agrees closely with the calculated values. The CCC and CCO in-plane and out-of-plane bending modes of these molecules are presented in Table 3. These findings were in correlation with the results discussed by our groups [26,27]. The other rocking, twisting and wagging deformations were identified with the aid of calculated vibrational frequencies of carvedilol in the present study.

4.3 UV spectral analysis

Electronic transition energies and oscillator strengths of carvedilol were calculated employing both the ZINDO and TD-DFT methods for which AM1-optimised geometries were used. The results of the ZINDO and TD-DFT calculations of electronic transition energies along with the band assignments are presented in Table 4, and they were compared with the experimental data of carvedilol in *n*-hexane. The present experiment revealed two bands at 238.6 and 203.6 nm in the UV region. The experimental and theoretical studies on the electronic absorption spectrum of carvedilol were made to explain each observed band, which was not done earlier. Both the theoretical methods (ZINDO and TD-DFT) typically overestimate the observed electronic band of carvedilol. The experimental electronic absorption bands were not well predicted by both ZINDO and TD-DFT calculations. However, the TD-DFT calculation fairly agrees with the experimental result than that of the ZINDO calculation. The HOMO–LUMO and HOMO–LUMO+1 band were predicted to be at 257 and 220 nm, respectively, by the TD-DFT calculation, which are fairly close to the observed 238.6 and 203.6 nm bands. Hence, the TD-DFT method appeared to be a better computational method to calculate the experimental bands of carvedilol.

Table 4. Assignment of observed electronic transitions.

Method	Energy (eV)	UV (nm)	Oscillator strength	Orbital
Experimental peaks[a]		238.6 203.6		
TD-DFT	4.21	294.5	0.0791	H-0- > L + 0(+71%) H-2- > L + 2(12%) H-2- > L + 0(+10%)
	4.59	269.9	0.13	H-2- > L + 0(+57%) H-0- > L + 2(+19%) H-0- > L + 0(9%)
	4.69	264.1	0.0001	H-1- > L + 0(+96%)
ZINDO	3.89	319	0.0474	H-1- > L + 0(+38%) H-0- > L + 1(+31%) H-0- > L + 0(18%)
	4.05	306.2	0.2339	H-0- > L + 0(+62%) H-1- > L + 0(+14%) H-0- > L + 1(+7%) H-1- > L + 1(6%)
	4.37	284	0.0003	H-0- > L + 4(+47%) H-3- > L + 0(23%) H-1- > L + 5(12%) H-6- > L + 1(6%)

[a] Solvent is *n*-hexane.

4.4 NMR spectral analysis

The ^{1}H NMR spectrum simulated theoretically with the aid of ChemDraw Ultra 8.0 is shown in Figure 4. Table 5 gives the ^{1}H NMR predicted chemical shift values obtained by the DFT method and ChemDraw Ultra 8.0 software program [28] and its assignments along with the experimentally obtained chemical shift values. The predicted shielding values for each atom in the carvedilol molecule by B3LYP/6-31G (d,p) are given in Table 5. However, the experimental study reports that the shielding constants are usually shifted relative to a standard compound, often tetramethylsilane. In order to obtain the theoretically predicted chemical shifts, its absolute shielding value is substracted from that of the reference molecule. In general, highly shielded electrons appear at downfield and vice versa. The predicted chemical shift values by the ChemDraw Ultra software program are in good agreement with the experimental chemical shift values than the values obtained by the DFT method.

The spectrum of carvedilol showed a singlet at 2.0 ppm for the proton of the alcohol (H_{36}) and amine (H_{37}) groups, which is in good agreement with the experimental chemical shift values of δ 1.8 ppm [6]. Though these two hydrogen atoms possess the same chemical shift values, the H_{37} hydrogen atom is more shielded than the H_{36} atom. Another singlet is predicted at δ 3.73 ppm for the methyl group hydrogen atoms (H_{46}, H_{47} and H_{48}). This higher chemical shift for methyl group hydrogen is mainly due to the oxygen atom (O_{15}) attached with the carbon atom (C_{16}). The predicted value of singlet peak at higher chemical shift of $\delta = 10.1$ ppm marks the indole proton (H_{49}). Two doublet peaks at $\delta = 7.4$ and 7.0 ppm appear due to four protons on the benzene ring adjacent to the indole ring. The multiplets in the region $\delta = 6.66$–6.97 ppm are due to seven protons of the two benzene rings of a similar environment. The hydrogen atoms attached with C_7 and C_1 atoms show a multiplet at $\delta = 4.0$ ppm, which is due to the presence of oxygen and nitrogen atoms at α and β positions, respectively. The hydrogen atoms attached with C_6 and C_3 atoms show a multiplet

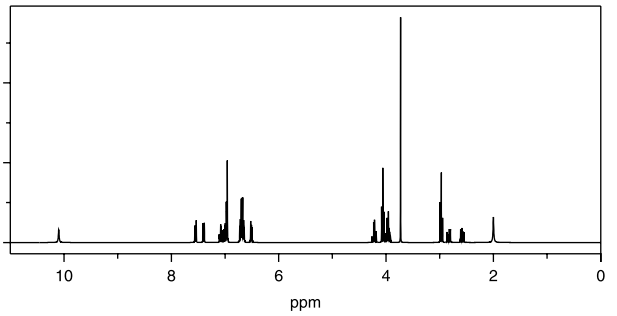

Figure 4. Theoretical ^{1}H NMR spectrum of carvedilol.

Table 5. Calculated and experimental proton NMR chemical shifts for carvedilol.

		Calculated chemical shift (ppm)		
Hydrogen atoms	Absolute shielding	B3LYP/6-31G(d,p)	ChemDraw Ultra	Experimental chemical shift (ppm) [6]
H_{31}	27.4398	5.16	4.22	4.2
H_{32}	27.2414	5.36	3.97	4.2
H_{33}	26.7832	5.81	3.96	4.2
H_{34}	28.0975	4.50	2.83	3.1
H_{35}	28.3350	4.26	2.58	3.1
H_{36}	29.4670	3.13	2.0	1.8
H_{37}	32.2827	0.32	2.0	1.8
H_{38}	28.0538	4.54	2.97	3.1
H_{39}	26.4427	6.15	2.97	3.1
H_{40}	26.4600	6.14	4.06	4.2
H_{41}	27.4648	5.13	4.06	4.2
H_{42}	24.3754	8.22	6.66	6.9
H_{43}	24.4915	8.11	6.71	6.9
H_{44}	24.5026	8.10	6.71	6.9
H_{45}	24.3255	8.27	6.66	6.9
H_{46}	27.2115	5.39	3.73	3.8
H_{47}	27.8024	4.80	3.73	3.8
H_{48}	26.1159	6.48	3.73	3.8
H_{49}	25.4682	7.13	10.1	8.2
H_{50}	24.6618	7.94	6.96	7.1
H_{51}	24.2181	8.38	6.97	6.7
H_{52}	24.8767	7.72	6.51	8.3
H_{53}	23.2661	9.33	7.55	7.4–7.2
H_{54}	24.2832	8.31	7.00	7.4–7.2
H_{55}	24.1653	8.43	7.09	7.4–7.2
H_{56}	24.3500	8.25	7.4	7.4–7.2

Table 6. Condensed Fukui functions (10^{-2}) from the NPA and MPA schemes.

	NPA		MPA	
Atoms	f_k^{+2}	f_k^{-2}	f_k^{+2}	f_k^{-2}
C_1	0.02025	0.13924	0.26569	0.18496
C_2	0.12996	0.00169	0.07921	0.36100
C_3	0.57121	0.00001	0.07569	0.02704
O_4	0.09409	0.28224	0.07569	0.58564
N_5	64.31296	0.02116	12.1000	0.05329
C_6	0.35721	0.00729	0.07921	0.01444
C_7	0.05929	0.00001	0.04624	0.25281
O_8	0.24964	0.38809	0.48841	0.00900
C_9	0.08281	0.01156	0.88804	0.61504
C_{10}	0.51076	0.07921	2.68324	0.47089
C_{11}	1.73889	0.76729	0.20736	0.22201
C_{12}	1.08241	0.18496	0.03025	0.00100
C_{13}	0.24649	0.21904	0.00784	0.21025
C_{14}	0.06724	4.84416	0.09216	0.82369
O_{15}	0.17424	0.33124	0.26896	0.00100
C_{16}	0.24336	0.00784	0.32761	0.97344
O_{17}	0.95481	2.06116	0.13456	0.61504
N_{18}	2.36196	2.24676	0.27889	1.06929
C_{19}	0.02116	0.23716	0.01369	4.50241
C_{20}	2.72484	0.82944	0.65536	1.16281
C_{21}	0.01296	11.0670	0.00064	1.60801
C_{22}	5.88289	2.90521	1.47456	1.02400
C_{23}	0.12321	10.9202	2.39121	11.9683
C_{24}	0.01156	1.74724	2.91600	1.70569
C_{25}	0.07056	1.67281	0.11664	0.80656
C_{26}	0.01521	8.17216	0.02209	1.96249
C_{27}	1.41376	0.04761	0.05329	0.03249
C_{28}	0.10404	7.77924	0.00841	1.32496
C_{29}	0.68644	1.95364	0.28900	1.56816
C_{30}	0.14161	0.04900	0.35721	2.86225

at $\delta = 2.6$ ppm, which may be due to the presence of oxygen and nitrogen atoms at β and α positions, respectively, and may reduce the chemical shift values.

4.5 Chemical reactivity

DFT is one of the important tools of quantum chemistry to understand popular chemical concepts such as electronegativity, electron affinity, chemical potential and ionisation potential [29]. The electron density-based local reactivity descriptors such as Fukui functions were proposed to explain the chemical selectivity or reactivity at a particular site of a chemical system [30]. Electron density is a property that contains all of the information about the molecular system and plays an important role in calculating almost all these chemical quantities. Parr and Yang [31] proposed a finite difference approach to calculate Fukui function indices, i.e. nucleophilic, electrophilic and radical attacks. In order to solve the negative Fukui function problem, different attempts have been made by various groups [32–34]. Kolandaivel et al. [15] introduced the atomic descriptor to determine the local reactive sites of the molecular system. In the present study, the AM1-optimised molecular geometry was utilised in single-point energy calculations, which have been performed at the DFT for the anions and cations of the conformers using the ground state with doublet multiplicity. The individual atomic charges calculated by natural population analysis (NPA) and Mulliken population analysis (MPA) have been used to calculate the Fukui function. Table 6 shows the f_k^{+2} and f_k^{-2} values for the title molecule calculated by NPA and MPA gross charges at DFT level of theory with the basis set (B3LYP/6-31G(d,p)). In order to eliminate the negative Fukui function, we used the square of the Fukui function in the present study. It has been found that both NPA and MPA scheme methods predict that the carbon atom C_{23} has a higher f_k^{+2} value for electrophilic attack. Also, both the population analysis schemes show N_5 amine nitrogen atom as the reactive sites for receiving a nucleophile. Almeida et al. [11] concluded that the N_5 atom of the amino group is the preferred site for protonation. Based on the Fukui function values in the present work, we predict N_5 to be the most favourable reactive site for protonation where the hydrogen atoms of N_5 are involved in intramolecular hydrogen bonding with O_4. Even though the f_k^{+2} and f_k^{-2} values are numerically less, it should be worth noting that the values are positive and the ordering of the reactivity has not been changed in any cases.

Note

1. Presently, Registrar, Periyar University, Salem, India.

References

[1] W. Carlson and K. Oberg, *Clinical pharmacology of carvedilol*, J. Cardiovasc. Pharmacol. Ther. 4(4) (1999), pp. 205–218.

[2] M. Metra, S. Nodari, A. D'Aloia, L. Bontempi, E. Boldi, and L. Dei Cas, *A rationale for the use of β-blockers as standard treatment for heart failure*, Am. Heart J. 139(3) (2000), pp. 511–521.

[3] G. Feuerstein and R.R. Ruffolo, Jr., *Beta-blockers in congestive heart failure: The pharmacology of carvedilol, a vasodilating beta-blocker and antioxidant, and its therapeutic utility in congestive heart failure*, Adv. Pharmacol. 42 (1998), pp. 611–615.

[4] S. Capomolla, O. Febo, M. Gnemmi, G. Riccardi, C. Opasich, A. Carporotondi, A. Mortara, G. Pinna, and F. Cobelli, *β-blockade therapy in chronic heart failure: Diastolic function and mitral regurgitation improvement by carvedilol*, Am. Heart J. 139(4) (2000), pp. 596–608.

[5] F. Wiedemann, W. Kampe, and M. Thiel, *Carbazolyl-(4)-oxypropanolamine compounds and therapeutic compositions*, US patent, 4503067, 1985-03-05.

[6] W.-M. Chen, L.-M. Zeng, K.-B. Yu, and J.-H. Xu, *Synthesis and crystal structure of carvedilol*, Chin. J. Struct. Chem. 17(5) (1998), pp. 325–328.

[7] P.J. Oliveira, M.P.M. Marques, L.A.E. Batista de Carvalho, and A.J.M. Moreno, *Effects of carvedilol on isolated heart mitochondria: Evidences for a protonophoretic mechanism*, Biochem. Biophys. Res. Commun. 276 (2000), pp. 82–87.

[8] M.P.M. Marques, P.J. Oliveira, A.J.M. Moreno, and L.A.E. Batista de Carvalho, *Study of carvedilol by combined Raman spectroscopy and* ab initio *MO calculations*, J. Raman Spectrosc. 33(10) (2002), pp. 778–783.

[9] D.R.P. Almeida, D.M. Gasparro, T.A. Martinek, F. Fulop, and I.G. Csizmadia, *Resolution of carvedilol's conformational surface*

via gas and solvent phase density functional theory optimization and NMR spectroscopy, J. Phys. Chem. A 108(38) (2004), pp. 7719–7729.

[10] D.R.P. Almeida, D.M. Gasparro, L.F. Pisterzi, L.L. Torday, A. Varro, J.Gy. Papp, B. Penke, and I.G. Csizmadia, *Molecular study on the enantiometric relationships of carvedilol fragment A, 4-(2-hydroxy propoxy) carbazol, along with selected analogues*, J. Phys. Chem. A 107(29) (2003), pp. 5594–5610.

[11] D.R.P. Almeida, D.M. Gasparro, L.F. Pisterzi, L.L. Torday, A. Varro, J.Gy. Papp, and B. Penke, *Gas phase conformational basicity of carvedilol fragment B, 2(s)-1-(ethylammonium) propane-2-ol: An* ab initio *study on a protonophoretic of oxidative phosphorylation uncoupling*, J. Mol. Struct. (Theochem.) 631 (2003), pp. 251–270.

[12] D.R.P. Almeida, D.M. Gasparro, L.F. Pisterzi, J.R. Juhasz, F. Fulop, and I.G. Csizmadia, *Conformational dependent basicity of carvedilol fragment C: An* ab initio *study on the primary amine, amino ethoxy -2-methoxy-benzene*, J. Mol. Struct. (Theochem.) 666–667 (2003), pp. 557–580.

[13] Gaussian 03, Revision A.1, M.J. Frisch, G.W. Trucks, H.B. Schlegel, G.E. Scuseria, M.A. Robb, J.R. Cheeseman, J.A. Montgomery, Jr., T. Vreven, K.N. Kudin, J.C. Burant, J.M. Millam, S.S. Iyengar, J. Tomasi, V. Barone, B. Mennucci, M. Cossi, G. Scalmani, N. Rega, G.A. Petersson, H. Nakatsuji, M. Hada, M. Ehara, K. Toyota, R. Fukuda, J. Hasegawa, M. Ishida, T. Nakajima, Y. Honda, O. Kitao, H. Nakai, M. Klene, X. Li, J.E. Knox, H.P. Hratchian, J.B. Cross, C. Adamo, J. Jaramillo, R. Gomperts, R.E. Stratmann, O. Yazyev, A.J. Austin, R. Cammi, C. Pomelli, J.W. Ochterski, P.Y. Ayala, K. Morokuma, G.A. Voth, P. Salvador, J.J. Dannenberg, V.G. Zakrzewski, S. Dapprich, A.D. Daniels, M.C. Strain, O. Farkas, D.K. Malick, A.D. Rabuck, K. Raghavachari, J.B. Foresman, J.V. Ortiz, Q. Cui, A.G. Baboul, S. Clifford, J. Cioslowski, B.B. Stefanov, G. Liu, A. Liashenko, P. Piskorz, I. Komaromi, R.L. Martin, D.J. Fox, T. Keith, M.A. Al-Laham, C.Y. Peng, A. Nanayakkara, M. Challacombe, P.M.W. Gill, B. Johnson, W. Chen, M.W. Wong, C. Gonzalez, and J.A. Pople, Gaussian, Inc., Pittsburgh PA, 2003.

[14] S.I. Gorelsky, *SWizard program*, 2005. Available at http://www.sg-chem.net/

[15] P. Kolandaivel, G. Praveen, and P. Selvarengan, *Study of atomic and condensed atomic indices for reactive sites of molecules*, J. Chem. Sci. 117(5) (2005), pp. 591–598.

[16] S. Sagdine, F. Kandemirli, and S.H. Bayari, Ab initio *and density functional computations of the vibrational spectrum, molecular geometry and some molecular properties of the antidepressant drug steraline (Zoloft) hydrochloride*, Spectrochim. Acta A 66(2) (2007), pp. 405–412.

[17] V. Krishnakumar and S. Seshadri, *Scaled quantum chemical calculation and FT-IR, FT-Raman spectral analysis of 2-methyl piperazine*, Spectrochim. Acta A 68(3) (2007), pp. 833–838.

[18] T. Chithambarathanu, V. Umayorubaghan, and V. Krishnakumar, *Vibrational analysis of some pyrozole derivatives*, Indian J. Pure Appl. Phys. 41(11) (2003), pp. 844–848.

[19] R. Zwarich, J. Smolarck, and L. Goodman, *Assignment of out of plane vibrational modes in benzaldehyde*, J. Mol. Spectrosc. 38(2) (1971), pp. 336–357.

[20] N.B. Colthup, L.H. Daly, and S.E. Wiberley, *Introduction to Infrared and Raman Spectroscopy*, Academic Press, New York, 1964, pp. 74, 221, 226.

[21] K. Nakanishi and P.H. Solomon, *Infrared Absorption Spectroscopy*, 2nd ed., Holden-Day, Inc., San Francisco, CA, 1977, p. 20.

[22] D.N. Singh and R.A. Yadav, *Force fields for CHO substituted benzenes: I. Planar and non-planar modes of benzaldehyde*, Asian Chem. Lett. 2 (1998), pp. 65–73.

[23] D.N. Singh and R.A. Yadav, *Force fields for C≡N substituted benzenes. I. Force fields for benzonitrile*, Asian J. Phys. 6 (1997), pp. 369–377.

[24] D.N. Singh, J.S. Singh, and R.A. Yadav, *Force fields for CN substituted benzenes. II Planar and non-planar modes of the three isomeric dicyanobenzenes*, J. Raman Spectrosc. 28(5) (1997), pp. 355–362.

[25] R.M. Silverstein, G.C. Besslor, and T.C. Morril, *Spectrometric identification of organic compounds*, 4th ed., Wiley, New York, 1981.

[26] S. Gunasekaran, R. Thilak kumar, and S. Ponnusamy, *Vibrational spectra and normal coordinate analysis of diazepam, phenytoin and phenobarbitone*, Spectrochim. Acta 65A (2006), pp. 1041–1052.

[27] S. Gunasekaran and P. Abitha, *Fourier transform infrared and FT-Raman spectra and normal coordinate analysis of aminobenzoesaeure*, Indian J. Pure Appl. Phys. 43 (2005), pp. 329–334.

[28] Chem3D Ultra 8.0, Software available at Cambridgesoft.com, Cambridge, MA.

[29] P. Hohenberg and W. Kohn, *Inhomogenous electron gas*, Phys. Rev. 136 (1964), pp. B864–B871.

[30] W. Yang and R.G. Parr, *Hardness, softness, and the fukui function in the electronic theory of metals and catalysis*, Proc. Natl Acad. Sci. USA 82 (1985), pp. 6723–6726.

[31] R.G. Parr and W. Yang, *Density functional approach to the frontier-electron theory of chemical reactivity*, J. Am. Chem. Soc. 106 (1984), pp. 4049–4050.

[32] R.K. Roy, K. Hirao, S. Krishnamurthy, and S. Pal, *Mulliken population analysis based evaluation of condensed Fukui function indices using fractional molecular charge*, J. Chem. Phys. 115 (2001), pp. 2901–2907.

[33] P. Bultinck, R. Carbo-Dorca, and W. Langenaekar, *Negative Fukui functions: New insights based on electronegativity equalization*, J. Chem. Phys. 118 (2003), pp. 4349–4356.

[34] P. Butlinck and R. Carbo-Dorca, *Negative and infinite Fukui functions: The role of diagonal dominance in the hardness matrix*, J. Math. Chem. 34 (2003), pp. 67–74.